The photophysics of solution processable semiconductors for applications in optoelectronic devices

Abdu-Aguye, Mustapha

DOI:
10.33612/diss.111696164

Chapter 4

Understanding the performance of Perovskite Solar Cells:

How Microstructure & Electron Extraction Layers affect light-soaking

In this chapter, the effect of the active layer microstructure on the light soaking effect on an inverted perovskite solar cell composed of the mixed halide perovskite: $CH_3NH_3PbI_{3-x}Cl_x$ is established by comparing different morphologies obtained by varying spin coating conditions to obtain either a "compact" or "non-compact" morphology. In addition, a triethylene glycol (TEG) modified fullerene derivative: PTEG-1 (with a relatively high dielectric constant of 5.9) which exhibits similar energy levels to the commonly used ester-functionalised fullerene derivative: phenyl-C_{61}-butyric acid methyl ester: PCBM (with a lower dielectric constant of 3.9) is used to supress the effect of light-soaking.

This chapter is based on the publications:

[1] S. Shao, **M. Abdu-Aguye**, T. S. Sherkar, H.-H. Fang, S. Adjokatse, G. T. Brink, B. J. Kooi, L. J. A. Koster, M. A. Loi, *Adv. Funct. Mater.* **2016**, *26*, 8094.

[2] S. Shao, **M. Abdu-Aguye**, L. Qiu, L.-H. Lai, J. Liu, S. Adjokatse, F. Jahani, M. E. Kamminga, G. H. Ten Brink, T. T. M. Palstra, B. J. Kooi, J. C. Hummelen, M. A. Loi, *Energy Environ. Sci.* **2016**, *9*.

4.1 The effect of microstructure on trap-assisted recombination and light soaking

4.1.1 Introduction

Hybrid Perovskites (HP) have attracted great interest over the past decade as a promising class of materials for optoelectronic applications owing to the almost unprecedented rise in power conversion efficiencies (PCEs) of devices utilising them as absorber materials[1–5]. They possess several advantageous properties such as: (i) a tuneable, direct bandgap, paired with a high absorption coefficient, up to ~10^5 cm^{-1} in the visible, comparable to that of Silicon (Si) and Gallium Nitride (GaN) (ii) very high and balanced carrier mobilities, which allows for (iii) the ability to be processed by either relatively straightforward solution-based methods (such as spin-coating, blade coating etc.) or vapour assisted means and (iv) a remarkable tolerance to (electronic) defects when processed from solution.

Understanding the limitations to the working of hybrid perovskite solar cells (HPSCs) has been challenging due to a plethora of reasons including (a) differences in quality of materials reported in literature makes it hard to separate extrinsic properties from intrinsic material properties (b) there are several diverse materials (and combinations thereof), device architectures and recipes reported with varying degrees of efficacy for device applications and lastly (c) there are sometimes conflicting reports on similar materials. All these factors have complicated our understanding of the intrinsic material properties and how processing affects the operation of HPSCs viz charge recombination, the presence of mobile ions, and, the light-soaking effect.

Among the several important challenges that must be addressed before HPSC technology is ripe for commercialization, the so-called "light soaking" effect has been identified as one of the most important. Light soaking refers to a reversible instability in hybrid perovskite solar cell (HPSC) device performance whereby the PCE increases upon illumination, and later returns to its initial performance when it is either stored in the dark or after the illumination is removed. Some reports in literature cite improvements of PCE as high as 100% over light illumination periods spanning from 10 to 30 minutes[6,7], understandably, this phenomenon is unwanted in working devices.

Several hypotheses have been put forth to explain the light-soaking phenomenon such as trap filling/de-filling[8,9], localized doping at the electrodes[10], and changes in the perovskite band structure due to reorientation of the (organic) cation under light and bias[11]. In many of these reports – mobile ions, photogenerated charges, and trap states play different roles which are not fully agreed upon. When one considers the variety of processing techniques, recipes, and device architectures in these reports, it is difficult to draw clear conclusions.

While several different architectures abound in literature, planar perovskite solar cells (p-PSCs) remain the most popular due to their advantage as a simple low temperature technique for making devices. However, the performance of such devices is intimately tied to the obtained morphology, which reflects in the microstructure and crystallinity of the active layer[12–14]. So far, poor coverage and reduced crystallinity of perovskite layers is accepted to be a cause of sub optimal device performance. Fortunately, there is wide ranging expertise cross-fertilised from decades of research into organic electronics and dye-sensitised solar cells which have led to improvements in all aspects of device engineering[13–19] to optimise device performance.

Although these advances in understanding how processing conditions can be optimised for improved device performance, little effort has been expended to understanding how the microstructure, which is a consequence of these processing conditions affects charge recombination, light-soaking and therefore PCE in devices. To address this shortcoming, we designed a series of experiments using perovskite films of $CH_3NH_3PbI_{3-x}Cl_x$ with different microstructures (reflected in different grain sizes and grain boundary distributions) obtained by varying the spin-coating parameters during processing to obtain either a "compact" or "non-compact" morphology, with "fused grain boundaries" and "open grain boundaries" respectively. We correlate the performance to the obtained microstructure using a combination of atomic force microscopy (AFM), electron microscopy, (light intensity dependent) *J-V* characterization, fluorescence microscopy and spectroscopy. Further, we show that films with a compact microstructure (more fused grains) are less susceptible to trap assisted recombination and consequently do not exhibit a pronounced light-soaking compared to those with a non-compact microstructure.

4.1.2 Morphology of films of mixed halide perovskites

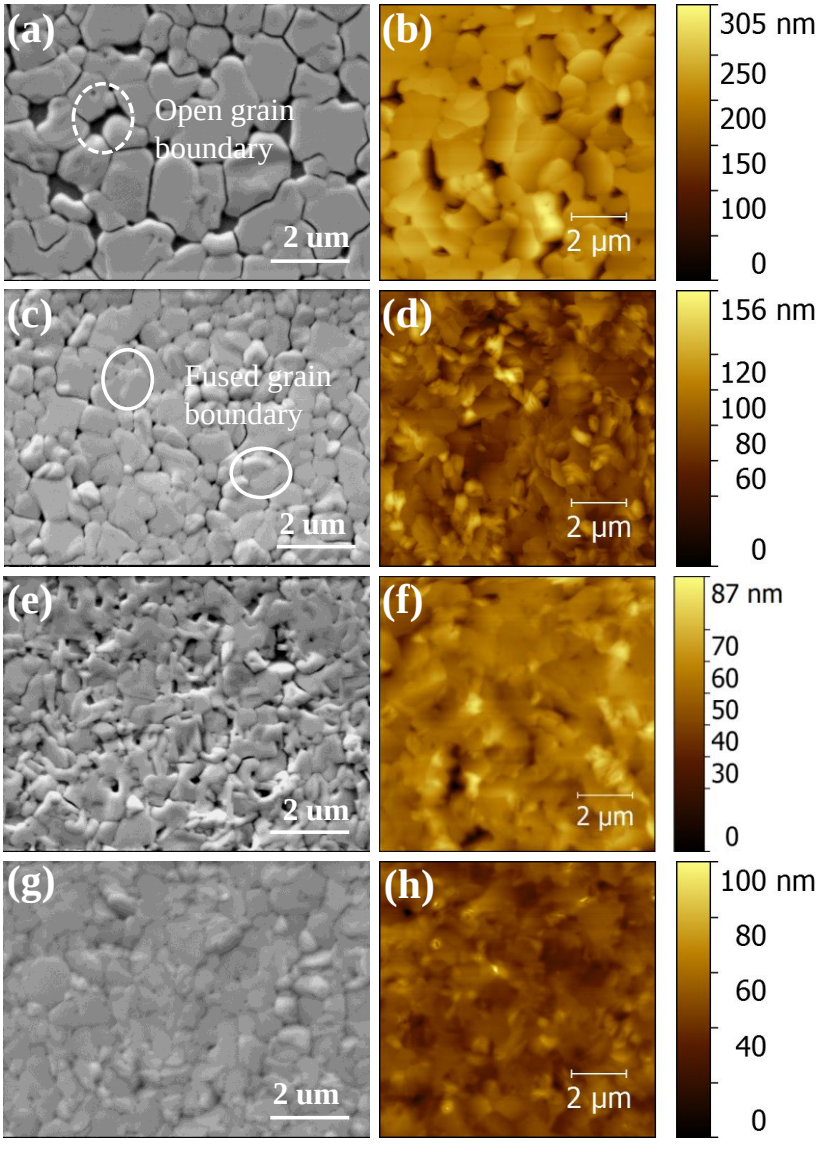

Figure 4.1: SEM and AFM topographic images for (a), (b) non-compact perovskite film; (c), (d) compact perovskite film; (e), (f) non-compact perovskite film with PCBM on top; (g), (h) compact perovskite film with PCBM on top

To produce perovskite films with different morphologies, films were spin coated at either 1,000 or 3,000 rpm. The fast evaporation of the solvent at high rotational speed promotes formation of a higher density of nucleation sites, which leads to small grain domains and thus, a denser perovskite polycrystalline film. Conversely, the relatively slower evaporation of the solvent during spin coating at a lower speed produces a lower number of nucleation sites, which grow into larger grains and result in a less compact film. To fabricate working devices, a 50nm thick layer of phenyl-C_{61}-butyric acid methyl ester (PCBM) is spin coated onto the perovskite layers.

To elucidate the final morphologies, scanning electron- and atomic force-microscopies were performed on these layers. Figure 4.1 above shows three important things; first, perovskite films cast at low spin speed display large micron-sized grains and holes as large as a few hundred nanometres in size, resulting in isolated grains with open grain boundaries. Secondly, films spin-coated at higher spin speeds result in a more compact morphology with smaller grains and more fused boundaries; as expected. Finally, when PCBM is deposited on the perovskite layers, the average roughness is drastically reduced to 9 nm & 4 nm respectively for non-compact and compact morphologies. This is likely a consequence of penetration of PCBM into the holes on the perovskite layers[20,21].

4.1.3 Photovoltaic Performance

To evaluate photovoltaic performance, p-i-n (p=p-type, i=intrinsic and n=n-type) planar device structure with layers: indium tin oxide(ITO)/hole extraction layer (HEL)/$CH_3NH_3PbI_{3-x}Cl_x$/electron extraction layer (EEL)/Al were fabricated. With poly(3,4-ethylenedioxythiophene):poly(styrene-sulfonate) (PEDOT:PSS) and PCBM as hole and electron extraction layers respectively. To study the effect of light-soaking, devices were kept illuminated at open-circuit in between scans (from -0.4 V to 1.4 V) and stored in the dark without any bias before measurements were carried out.

Figure 4.2 below shows the *J-V* scans for both devices before and after light soaking with a summary of all parameters in table 4.1 underneath. Devices fabricated from the non-compact perovskite films display a strong variation in photovoltaic performance upon light-soaking; with a very low initial performance (V_{oc} of 0.42 V, J_{sc} of 19.4 mA cm^{-2}, FF of 60% and PCE of 3.7%) which more than doubles after light-soaking for 1.5 hr (V_{oc} of 0.87 V, J_{sc} of 19.0 mA cm^{-2}, FF of 70% and PCE of

11.6%). On the other hand, devices made from the compact perovskite films display only weak dependence on light soaking with performance remaining mostly unchanged upon extended illumination (V_{oc} goes from 0.86 V to 0.88 V, J_{sc} from 18.4 mA cm^{-2} to 18.3 mA cm^{-2}, FF from 72% to 74%, and PCE slightly rises to 11.9% from 11.4%). It should be noted that the light soaking, in the former case, is fully reversible – the devices return very close to their initial performance after storage in the dark for 1.5hrs, and can be similarly improved upon a second round of light soaking. Another important detail to note is that the morphology of the devices is not changed upon light-soaking.

Despite the differences in initial device performance between the two samples, after light soaking, they display very similar V_{oc} and FFs (the slight difference in observed J_{sc} is likely due to small differences in absorption of the two films). This observation suggests that the light-soaking effect is dependent on the microstructure of the active layer of the film. The possibility of direct contact between PCBM and PEDOT:PSS is extremely low because the thickness of the perovskite layer exceeds the depth of the pinholes, and a control device with ITO/PEDOT:PSS/PCBM does not show any variation with light-soaking, excluding any changes in the PEDOT:PSS/PCBM junction as a source of the observed light soaking.

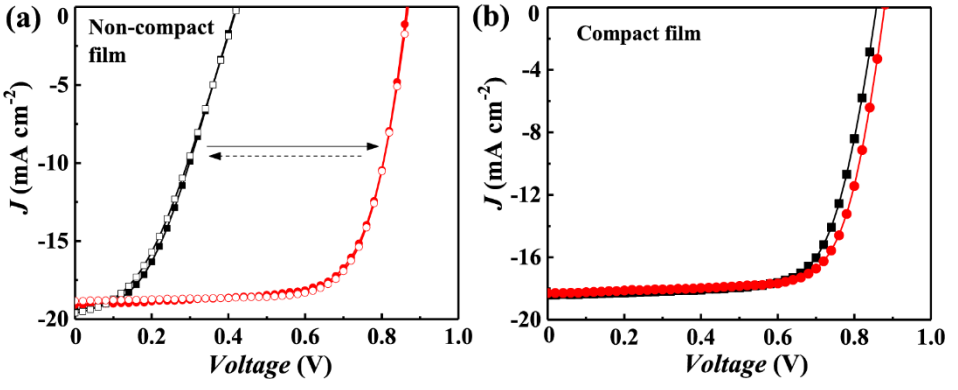

Figure 4.2: *J-V* curves of HPSCs using (a) non-compact and (b) compact perovskite film, measured before (solid square) and after light soaking (solid circle) under one sun illumination (the open square measured for the light soaked device after storage in dark for 1.5 h and the open circle measured after another round 1.5 h light soaking following the open square).

Further checks of (a) the photovoltaic performance under light soaking with an even more compact film yields virtually no dependence on extended illumination in agreement with the assertion that light-soaking is dependent on the microstructure

of the film, and (b) n-i-p planar devices with structure: fluorine-doped tin oxide (FTO)/EEL/$CH_3NH_3PbI_{3-x}Cl_x$ /HEL/Au (the EEL and HEL are TiO_2 and the small molecule based Spiro-OMETAD); in this case, severe light soaking is also observed in the non-compact film. In particular, these combined observations suggest that open boundaries are detrimental to device performance.

Device	V_{OC} (V)	J_{SC} (mA cm)	FF	PCE (%)
Non-compact perovskite [b]	0.42	19.4	0.46	3.7
Non-compact perovskite [a]	0.87	19.0	0.7	11.6
Compact perovskite [b]	0.86	18.4	0.72	11.4
Compact perovskite [a]	0.88	18.3	0.74	11.9

Table 4.1: Summary of the effect of the light soaking on the performance parameters of the devices using a 50 nm thick $PC_{60}BM$ layer as EEL (*b* and *a* represent the performance of devices before and after light soaking respectively)

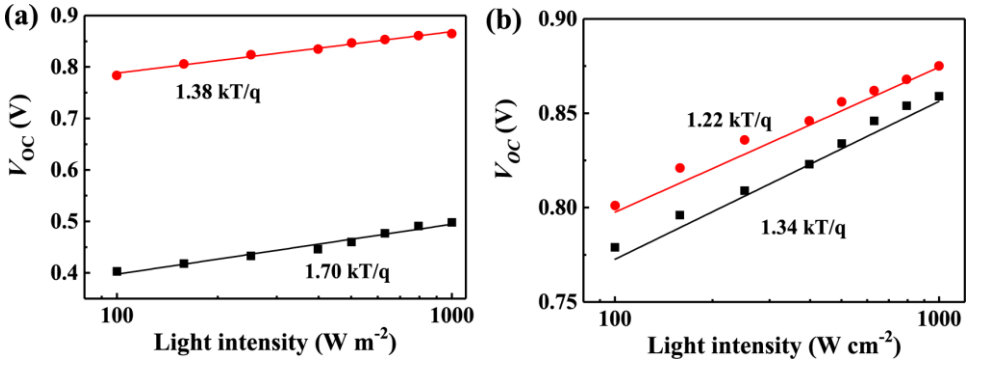

Figure 4.3: Light intensity dependent V_{OC} after (red) and before (black) light soaking for devices with (a) non-compact, (b) compact perovskite films.

4.1.2 Light intensity dependent J_{sc} and V_{oc} measurements

The light intensity dependence of the *Jsc* and *Voc* were measured in devices with compact and non-compact perovskite layers both before and after light soaking. To determine the effect of light intensity on the initial device performance, the experiments were carefully designed to minimize the effect of light soaking and the *J–V* curves were recorded every 1.5 h between each measurement at different light intensity.

During these 1.5 h intervals, the devices were stored under dark conditions to return to their initial state. To determine the effect of light intensity on the light soaked device performance, the *J–V* curves were measured on a soaked device sequentially under varied light intensity without any extra storage in the dark. The J_{sc} of both samples under light-soaking is relatively stable as reflected in the semi-logarithmic plot of J_{sc} versus light intensity in the appendix of this chapter. The slope (representing the so-called alpha parameter) for both compact and non-compact morphologies before and after light-soaking is very close to 1 indicting that the amount of bimolecular recombination remains unchanged and thus, excludes it as a potential mechanism for light-soaking[21,22].

For light intensity dependent V_{oc} measurements on the other hand, from the slope of the semi-logarithmic plot of V_{oc} versus light intensity, the ideality factor (n) in units of KT/q can be determined as shown in Figure 4.3 above. The ideality factor is 1 in the absence of any trap-assisted recombination and deviates from 1 up to a value of 2 as trap-assisted recombination becomes more dominant in the active layer[22]. Before light-soaking, devices made from the non-compact perovskite layer have $n = 1.7$ compared to $n = 1.34$ for devices made from the compact perovskite layer; these values indicate the device with a non-compact morphology is characterised by a higher amount of trap assisted recombination due to a higher trap density at the open grain boundaries compared to the device with the compact morphology which has a reduced amount of traps as a result of having more fused grain boundaries.

After light-soaking, the ideality factors change to $n = 1.38$ and $n = 1.22$ respectively, this indicates that light-soaking effectively supresses trap assisted recombination in the non-compact perovskite layer, this agrees qualitatively with the weak dependence on light-soaking already observed in the devices with a compact perovskite layer. Therefore, we conclude that the devices made from the compact perovskite layer are characterised by a lower trap density due to the fused grain boundaries which leads to strongly reduced trap assisted recombination of the charge carriers in the active layer.

4.1.3 Spectroscopic Studies

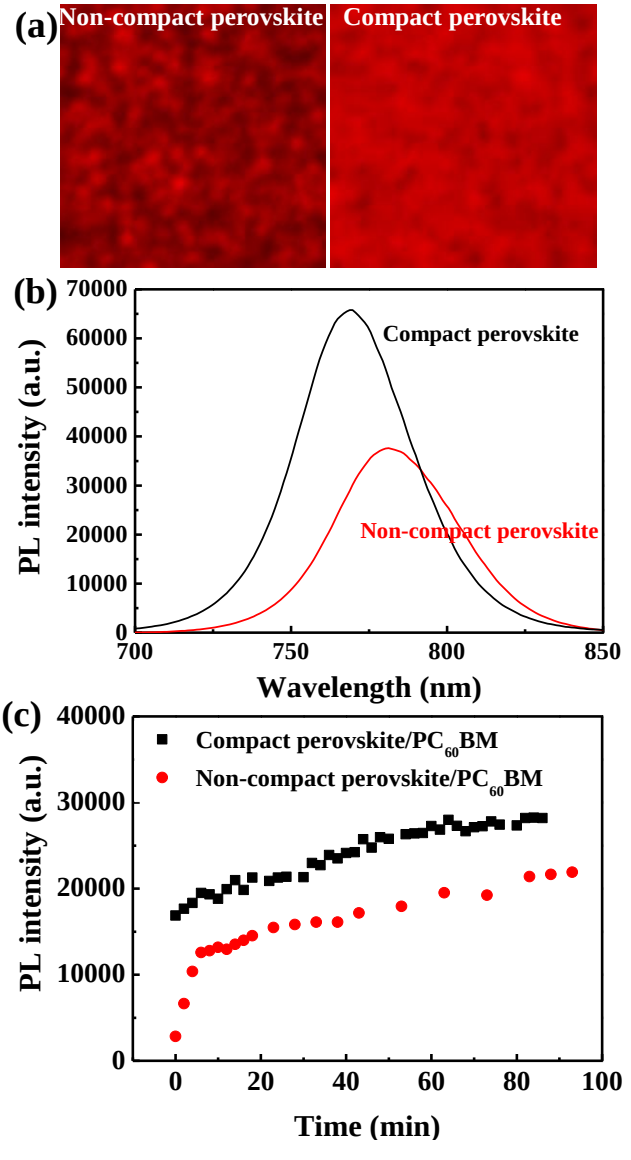

Figure 4.4: (a) Confocal microscopy images (20×20 μm) for non-compact and compact perovskite film, (b) steady state PL spectra for pristine non-compact and compact perovskite films, (c) the variation in the PL intensity of the perovskite film (non-compact and compact)/PCBM samples with light soaking time.

Turning attention to possible sources of traps which can explain the differences between photovoltaic device performance, it has been reported that hybrid perovskites may contain under-coordinated metal ions at crystal surfaces and also at grain boundaries between individual crystals which lead to halide vacancy defects that act as electron traps[23]. Additionally, a few theoretical reports have identified the small formation energies of such halide defects to be the reason why they are so abundant in perovskite films[24,25].

Figure 4.4(a) above shows confocal photoluminescence (PL) micrographs for the compact and non-compact perovskite films taken in ambient conditions with constant excitation and image acquisition parameters. Previous studies have suggested that shallow traps contribute to radiative recombination while deep trap states produce non-radiative recombination[19]. The non-compact perovskite film shows inhomogeneous emission, implying a non-uniform distribution of deep trap states while regions in proximity of the open grain boundaries emit weakly. This can be due to the accumulation of deep traps, probably caused by iodide vacancies at the interfaces between grain boundaries. The PL intensity not only varies from grain to grain but also within the grains due to variation in the quality of the individual crystals.

Conversely, the compact perovskite film shows brighter and more homogeneous emission. This indicates that in the fused grain boundaries of the compact perovskite film, the density of deep trap states is dramatically reduced. Therefore, we speculate that the open grain boundaries of the non-compact film are characterized by a high density of deep trap states and that fused grain boundaries help to eliminate these deep trap states in the perovskite film. This is further confirmed by photoluminescence measurements, showing that the compact perovskite film has much higher PL intensity and its peak emission shifts toward shorter wavelengths in comparison to the non-compact perovskite film. These results also explain the weak dependence of the device performance of the compact layer (small grains) device on light soaking.

Further exploring the effect of light-soaking after the deposition of a 50 nm thick PCBM EEL, The non-compact perovskite film shows a fast increase in PL intensity within the first 30 mins and then slowly saturates in about 1.5 h of light soaking. The rise in PL intensity is attributed to a trap-filling process occurring with light soaking. In contrast, the compact perovskite film shows only a minor improvement in the PL intensity over the same period of illumination. The enhanced PL intensity

with light soaking of the non-compact perovskite film suggests a high trap density in the perovskite film even after deposition of PCBM; therefore, the PL results highlight that the light soaking phenomenon is dominated by trap-assisted recombination. The similar trend for the PL intensity in the perovskite films and the device performance suggest the same underlying mechanism. When traps are filled under continuous light soaking, the larger splitting in the quasi-Fermi energy levels leads to an enhanced V_{oc}. In the meantime, free charge carriers are extracted more easily to the EEL, leading to enhanced fill factor and PCE.

4.1.4 Conclusion

In conclusion, we have investigated how the grain boundaries and grain size in perovskite films affect the charge recombination and light soaking effect in hybrid perovskite solar cells. We find that interface trap-assisted recombination dominates the light soaking effect. The devices made with a compact perovskite film show a very weak light soaking effect due to lower trap-assisted recombination, while those made with a non-compact perovskite film show a strong light soaking effect due to significant trap-assisted recombination. Our results demonstrate that improving the morphology of the perovskite film to eliminate the grain boundaries is an effective way to eliminate the light soaking effect to obtain more stable device performance from hybrid perovskite solar cells.

4.2 Enhancing the performance of perovskite solar cells using a high-ε_r fullerene derivative as electron extraction material

4.2.1 Introduction

Next to the microstructure of the active layer, charge transport layers can also play an important role in light-soaking phenomenon and the eventual device performance in HP solar cells. In this work, we investigate how electron extraction layers (EELs) with different dielectric constants affect the device performance and the light-soaking phenomenon in hybrid perovskite solar cells (HPSCs). As shown earlier, trap states in HP layers are responsible for the light soaking effect, in agreement with work by other authors[8]. In addition, reports by other authors have pointed to various other possibilities as the origin for light-soaking in HPSCs such as surface traps in TiO_2 EEL[16,26], the interaction between charges accumulated at

electrodes and positively charged traps in the bulk of the HP layer[27], and a "doping" mechanism driven by charge accumulation at electrodes[10].

Another line of inquiry in recent computational studies have identified HP layers as being very prone to defects including vacancies, interstitial atoms, substituent atoms, and grain boundaries in the crystal structure[19,24,28,29]. These defects in HP absorber layers are believed to play a critical role in determining the V_{oc} of a solar cell. Defects that create deep energy levels usually act as recombination centres resulting in non-radiative trap assisted recombination which lead to low V_{oc} Whereas, defects acting as shallow levels are benign to device performance[19]. While the nature of traps in CH_3NH_3I-based HPs is still unclear, there have been a host of studies, both experimental and theoretical, asserting that both deep and shallow traps abound, however, more importantly, a recent report showing surprisingly low trap density in HP single crystals points towards material quality as playing a role in determining the trap density[30].

An additional point of consideration, which while well researched in organic solar cells[31], has gone mostly unaddressed in the HP literature, is the effect of the dielectric constant (ε_r) on device performance. HPs have high dielectric constants with reported values higher than 6.5, which leads to very small binding energy of electron–hole pairs and generation of free carriers upon excitation[4,32–34]; However, many organic charge carrier extraction layers, for example, PCBM, usually feature a relatively low dielectric constant (~3.9). This dielectric mismatch has been shown to be unfavourable for charge separation at the heterojunction interface[35,36].

Here, we investigate the effects of the dielectric constant of the EEL on the trap assisted recombination and light-soaking phenomena in HPSCs. We use a triethylene glycol monoethyl ether side chain substituted fulleropyrrolidine (PTEG-1) having a dielectric constant of 5.9[37,38] as an EEL in HPSCs. The commonly used fullerene derivative PCBM, which has identical energy levels but a lower dielectric constant of ~3.9, is used as a reference. The device using PTEG-1 as the EEL shows a negligible light soaking effect, with a power conversion efficiency (PCE) of 15.2% before light soaking and a minor increase to 15.7% after light soaking.

In contrast, the device using PCBM as the EEL shows severe light soaking, with the PCE improving from 3.8% to 11.7%. Photoluminescence (PL) measurements indicate that trap-assisted recombination at the interface between the hybrid perovskite and the EEL can also cause the light-soaking effect in HPSCs. The trap-

assisted recombination is effectively suppressed at the perovskite/PTEG-1 interface, while severe trap assisted recombination takes place at the perovskite/PCBM interface. We attribute these experimental findings to the fact that the higher dielectric constant of PTEG-1 helps to screen the recombination between the traps and free electrons. In addition, the electron donating side chains of PTEG-1 may also contribute to the passivation of the electron traps. As a consequence, the devices using PTEG-1 as the EEL display a considerable increase in the efficiency and a negligible light soaking effect.

4.2.2 Photovoltaic device performance & morphology

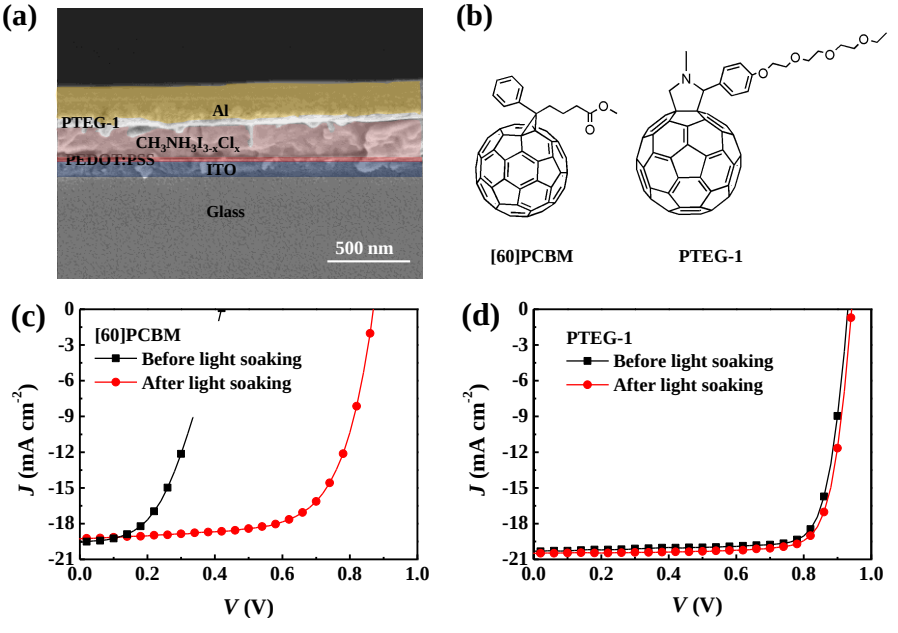

Figure 4.5: (a) Cross sectional SEM image of the device architecture, (b) chemical structures of PCBM and PTEG-1, *J-V* characteristics under illumination for the devices using (c) PCBM and (d) PTEG-1 as EEL.

As in the former section, p-i-n planar HPSCs were fabricated with a similar structure: ITO/ PEDOT:PSS/$CH_3NH_3PbI_{3-x}Cl_x$/EEL/Al; with either PTEG-1 or PCBM as the EEL (see chemical structures in Figure 4.5(b)). The performances of the devices using these two different EELs were then investigated under continuous illumination.

Before measurement, the devices were stored in the dark without any external bias. Hereafter, the condition under which the devices are measured immediately after

exposure to the AM 1.5G spectrum of a solar simulator is termed 'before light soaking' and the condition under which the device is measured after reaching saturation in performance with exposure to light is termed 'after light soaking'. Figure 4.5 above shows the *J-V* characteristics of two representative devices with either a PTEG-1 or PCBM EEL, both before and after light-soaking. The reference device, with a PCBM EEL, shows very poor performance before light soaking (V_{oc} = 0.42 V, J_{sc} = 19.50 mAcm^{-2}, FF = 0.46 and PCE = 3.8%); which increases upon 1.5hrs of light-soaking (V_{oc} = 0.87 V, J_{sc} = 19.20 mAcm^{-2}, FF = 0.70 and PCE = 11.7%). The PTEG-1 based device on the other hand, shows a much weaker dependence on light soaking with initial performance (V_{oc} = 0.93 V, J_{sc} = 20.40 mAcm^{-2}, FF = 0.80 and PCE = 15.2%) remaining very close to what is observed after light-soaking (V_{oc} = 0.94 V, J_{sc} = 20.63 mAcm^{-2}, FF = 0.81 and PCE = 15.7%). The device parameters are summarized in table 4.2 below.

Device	V_{OC} (V)	J_{SC} (mA cm^{-2})	FF	PCE (%)
PCBM [a]	0.42	19.50	0.46	3.77
PCBM [b]	0.87	19.20	0.70	11.69
PTEG-1 [a]	0.93	20.40	0.80	15.18
PTEG-1 [b]	0.94	20.63	0.81	15.71

Table 4.2: Summary of device performance for the PCBM and PTEG-1 based HPSCs (the superscripts *b* and *a* represent the device performance before and after light soaking respectively)

Interestingly, it should be noted that regardless of light soaking, the PTEG-1 based device performs better than the PCBM-based one. The next Figure, 4.6, shows the evolution of the photovoltaic parameters of the devices under illumination with time from which it can be observed that the increase in PCE of the PCBM-based device is explained by an increase in the V_{oc} and FF over a time scale of 1.5 hrs; with an initial rapid rise taking about 0.5 hr followed by a more gradual increase over the remaining hour.

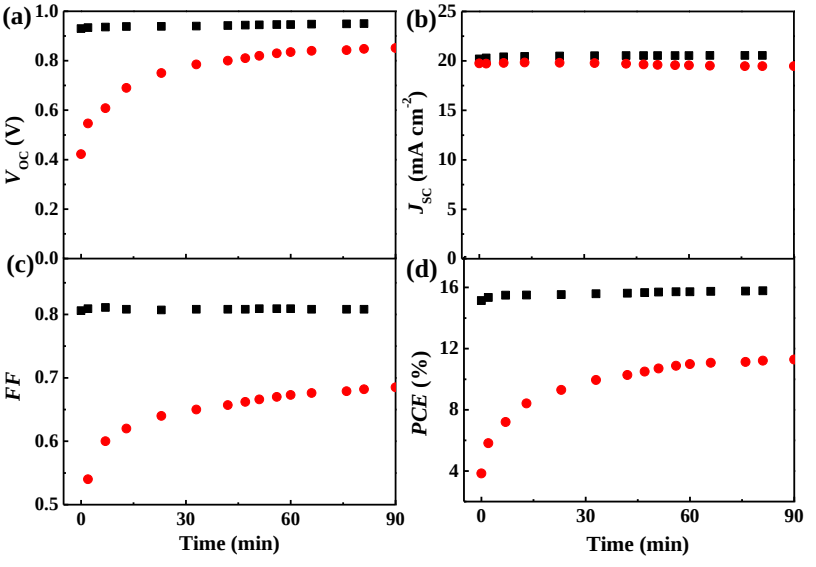

Figure 4.6: Time evolution of the (a) V_{OC}, (b) J_{SC}, (c) FF and (d) PCE of the device using PTEG-1 and PCBM as EEL under illumination.

4.2.3 The origin of light-soaking: trap-assisted recombination

To explore the origin of the light-soaking effect in the HPSCs fabricated, we performed light intensity dependent *J-V* measurements as before; observing as mentioned earlier, that the phenomenon is fully reversible i.e. devices regain their initial performance upon storage in the dark for 1.5 hr. Devices measured before light soaking were measured under varied light intensity with an interval of 1.5 hr between each measurement; during the interval the devices were stored in a nitrogen filled glove box in the dark to return to their original state. For the devices measured after light soaking, the *J–V* curves were measured sequentially without any extra storage in the dark.

Like before, light-soaking does not have any discernible effect on the J_{sc} of both types of devices, their so-called alpha parameters both remain 1 which indicates that bimolecular recombination is not dominant[39] and can therefore not be invoked as a reason for the light-soaking. On the other hand, light intensity dependent V_{oc} measurements shown in Figure 4.7 below give a clue as to the origin of improvements in device performance[40].

The ideality factor, n, of the reference PCBM device decreases from an initial value of 1.70 before light-soaking to 1.38 afterwards; while the PTEG-1 based device has n = 1.23 before light-soaking which reduces to 1.18 after being light-soaked. The reference device initially suffers from a significant energy loss from trap-assisted recombination which decreases upon light-soaking in agreement with the *J-V* measurements. Also, the comparatively lower value of n in the PTEG-1 based device suggests that PTEG-1 alleviates trap-assisted recombination more effectively than PCBM. These observations therefore point towards trap-assisted recombination as the source of the light-soaking effect observed in the *J-V* measurements.

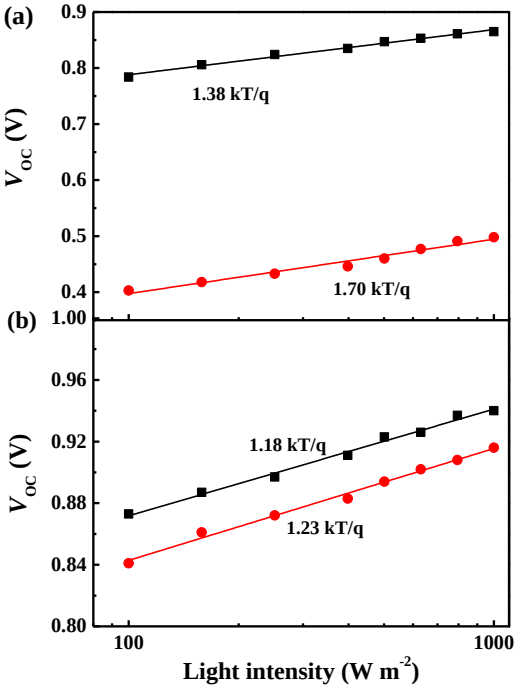

Figure 4.7: Light intensity dependent V_{OC} for the devices using (a) PCBM and (b) PTEG-1 as EEL before light soaking (in red) and after light soaking (in black). Symbols are experimental data and lines are the result of linear fitting.

To further understand the nature of these traps, steady-state and time-resolved PL measurements were performed on the HP films. Steady state PL measurements were performed in transmission mode on samples with a structure of ITO/PEDOT:PSS/HP/EEL, which were prepared under identical conditions to those for the solar cells. Figure 4.8(a) shows the variation in PL intensity recorded

at the peak emission (780 nm) of the HP film excited at 400 nm at 295 K in a N_2 atmosphere. The HP film with PCBM as the EEL shows a large and rapid increase in PL intensity within the first 0.5 hr of exposure to laser illumination and then saturates in about 1.5 hrs. In contrast, the HP film with PTEG-1 as the EEL shows only minor improvement in PL intensity over the same illumination time.

It is important to underline that the rise time of the PL intensity matches that of the photo-voltage. It is also noted that HP/PTEG-1 samples emit light more effectively than the HP/PCBM samples. The PL data thus confirm that the deep electron trap-assisted recombination dominates the light soaking phenomenon; furthermore, the comparably slow photo-response of the performance of both devices and the comparably slow variation of the PL could be an indication of trap filling by mobile ions. This hypothesis was tested by temperature dependent V_{oc} measurements on devices with a PCBM EEL, which showed that the increase in V_{oc} is much slower at lower temperatures after 1.5 hr of light soaking; implying that the trap-filling process is deactivated at lower temperatures. Time-resolved PL measurements provide deeper insight into the influence of the trap states on the radiative decay dynamics. Figure 4.8(b) shows the time-resolved PL decay measurements, taken at 780 nm measured at room temperature.

The pristine HP layer exhibits a mono-exponential PL decay with a lifetime of about 7.6 ns. When PCBM and PTEG-1 are deposited on it, the PL decay becomes bi-exponential. A faster decay is measured for the sample with PCBM, which shows a pronounced fast component with a lifetime of 0.9 ns and a weaker component with a lifetime of about 11 ns. The PTEG-1 sample shows two components of similar intensity and with lifetimes of 1.9 ns and 5 ns. These experimental results indicate that the charge transfer process is much faster than the charge recombination process in the HP layer. Though the electron transfer from the HP layer to PCBM appears to be more efficient than that of PTEG-1, the HPSCs using the PCBM EEL suffers more severe trap-assisted recombination than the devices based on PTEG-1. Obviously, severe trap-assisted recombination opens up a new deactivation channel that should be evident in the dynamics of photoluminescence, explaining the faster decay time of the sample containing PCBM compared to PTEG-1.

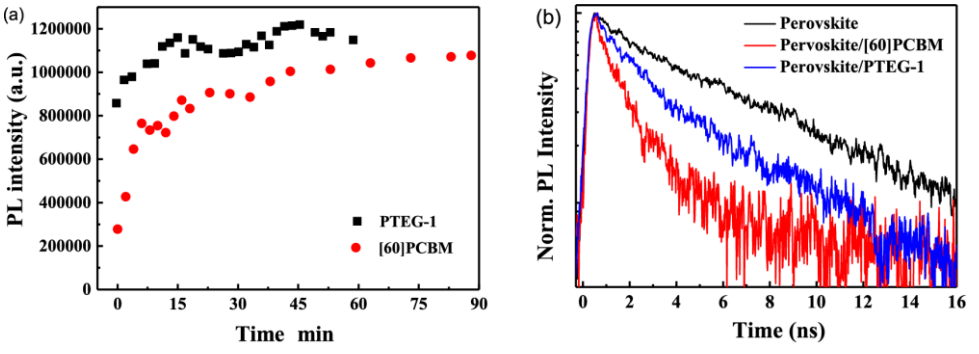

Figure 4.8: Variation of the PL intensity (detected at 780 nm) for perovskite/PTEG-1, and perovskite/PCBM (b) Time resolved PL before light soaking for pristine perovskite (black line), perovskite/PCBM (red line), and perovskite/PTEG-1 (blue line).

4.2.4 Mechanism of trap-assisted recombination suppression

As mentioned in the previous section, iodine vacancies have the lowest formation energy which enable anion (I^-) migration with a relatively low activation energy of about 0.6 eV[24,25,28]. Therefore, it is likely that the positively charged iodine vacancies (V_I^+) act as electron traps in HPSCs and the mobile I^- anions can fill them during light soaking. From a molecular design perspective, we can discuss the possible mechanism for the reduced light soaking effect as follows:

The Figure 4.9(a) below depicts the trap-assisted recombination process occurring between the perovskite layer and the EEL. The photogenerated electrons are first injected into the EEL and pile up at the perovskite/EEL interface before being collected at the cathode. These accumulated electrons can be captured by surface traps in the perovskite layer before being collected at the cathode; ending up recombining non-radiatively. We propose that the capture of electrons by interface traps is driven by the Coulombic interaction between the electrons and the positively charged trap states on the perovskite surface. There is therefore, a critical distance (r_c) at which the charges can escape the electrostatic force of these traps with the aid of available thermal energy (KT) – this distance can be expressed as follows[35]

$$r_c = \frac{q^2}{4\pi\varepsilon_0\varepsilon_r KT} \qquad (4.1)$$

Where q, T, ε_0 and ε_r are respectively the elementary charge, temperature, vacuum permittivity and dielectric constant of the EEL. Electrons in the EEL that are within

the critical distance thus have a high probability to be trapped[4]. It is obvious that increasing the ε_r of the EEL reduces the r_c value and therefore supresses the trap-assisted recombination.

Previous studies have pointed out that the flexible oligoethylene oxide chains give rise to a high (molecular) polarizability and thus a higher ε_r for PTEG-1 compared to PCBM[37,38]. At 295K, the r_c value for the PCBM based device is 15.2 nm compared to 9.5 nm for the PTEG-1 based device. Therefore, PTEG-1 more effectively screens the electrostatic force and supresses the trap-assisted recombination in the solar cells. This explains the reduced light soaking effect and enhanced performance of the PTEG-1 based HPSCs. The temperature dependence of the V_{oc} in HPSCs using both EELs is shown in Figure 4.9(b).

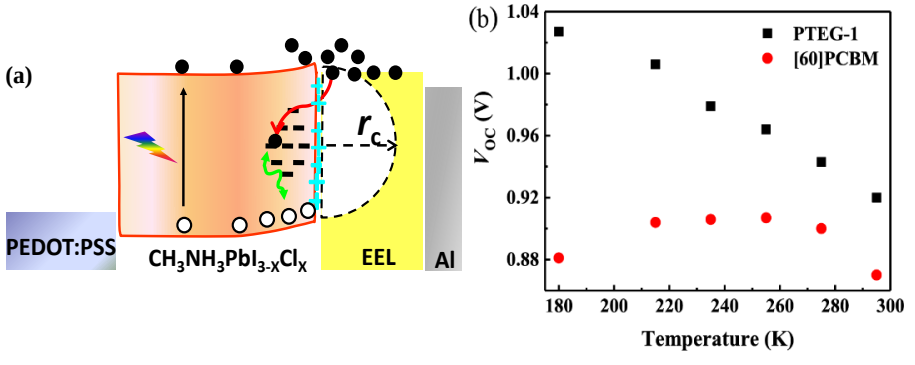

Figure 4.9: (a) Schematic of the proposed mechanism for the light soaking phenomenon, (b) V_{OC} measured after light soaking for the devices using PCBM and PTEG-1 as EEL at different temperatures.

Here, two interesting points to note are that the trap density in perovskite films are known to decrease as the temperature decreases[8,41] and the r_c values increase according to the equation 4.1 above.

For the PCBM-based HPSC, the maximum V_{oc} value is observed at 255 K; above which the trap-assisted recombination is dominated by the trap density and below which the increased electrostatic binding force between the charges dominates (r_c = 20 nm at 215 K). Thus, a trade-off between trap density and electrostatic binding force results in a maximum V_{oc} at 255 K. On the other hand, the PTEG-1 based HPSC shows a consistently increased V_{oc} as the temperature decreases from 295 K to 180 K.

Owing to the higher ε_r of PTEG-1 and assuming limited variation of it within the temperature range in question, the electrostatic force is not significantly increased even at low temperatures (r_c = 13 nm at 215 K), thus the increase in V_{oc} is due to a supressed recombination due to a reduction in the trap density at low temperatures. A further consideration to make is that PTEG-1 contains electron donating side-chains consisting of a tertiary amine and triethylene oxide moieties which may coordinate with the iodide vacancies and thus passivate the electron traps – in a similar fashion to reports on trap passivation by Lewis bases by Snaith and co-workers[42]. Therefore, the high-ε_r and electron donating properties of PTEG-1 may synergistically reduce the trap-assisted recombination and thus eliminate the light-soaking phenomenon in HPSCs.

4.2.5 Conclusion

In conclusion, we investigated how the EEL affects the device performance and light-soaking phenomenon in HPSCs. A high-ε_r (5.9) fullerene derivative (PTEG-1) was used as an EEL and compared to the most common fullerene derivative: PCBM, which also has a lower ε_r (~3.9). The PCE of HPSCs based on PTEG-1 is about 15.7% which is substantially higher than the 11.7% efficiency obtained using PCBM. What is also important is devices using PTEG-1 as the EEL show negligible light-soaking effect compared to those using PCBM, which are severely affected by light soaking. Using PL spectroscopy we identify surface electron trap assisted recombination plays a dominant role in the light soaking effect and thus strongly affects the device performance. The relatively high ε_r of PTEG-1 helps to screen the electrostatic force between the traps and free electrons in the EEL; in addition, the electron donating side chains of PTEG-1 may passivate the electron traps. These two factors may synergistically improve the charge collection and reduce the light soaking effect.

4.3 Experimental

4.3.1 Materials

CH_3NH_3I was purchased from Luminescence Technology Corporation. A PEDOT:PSS dispersion in water (Clevios VP AI 4083) was acquired from Heraeus. $PbCl_2$ (99.99%), N,N-dimethylformamide (DMF) (99.8%) and chloroform (99.8%) were acquired from Sigma-Aldrich.

4.3.2 Device Fabrication

ITO coated glass substrates were sonicated sequentially in detergent, deionized water, acetone and isopropanol for 20 minutes each respectively. After spin-drying, the clean substrates were further dried in at 140 ºC for 10 minutes to remove leftover solvents. Afterwards, a UV-ozone cleaning treatment was performed on the substrates for 20 minutes after which an approximately 30nm thick PEDOT:PSS layer was spin-coated onto them and subsequently dried for another 10 minutes at 140 ºC. A precursor solution (40wt%) of CH_3NH_3I and $PbCl_2$ in a 3:1 molar ratio was then spin-coated onto the PEDOT:PSS layer and then immediately stored under high vacuum (<10^{-6} mbar) for 12 h. Afterwards the layers were annealed at 100 ºC for 1h in a nitrogen-filled glove box. In this manner either 280 nm thick or 210 nm thick (in the non-compact case) films of $CH_3NH_3PbI_{3-x}Cl_x$ were obtained. Next, a 50 nm thick EEL was spin-coated onto the perovskite layer. The devices were completed by evaporating a 100 nm thick Al layer under high vacuum (<10^{-6} mbar)

4.3.3 Solar Cell Characterization

Current density-voltage characteristics of the solar cells were measured under simulated AM 1.5G solar illumination using a Steuernagel Solar constant 1200 metal halide lamp in a nitrogen-filled glove box. The light intensity was calibrated to be 100 mW cm^{-2} using a calibrated Si cell.

4.3.4 Photoluminescence Measurements

Samples for PL measurements were prepared in the same way as the devices but without the deposition of the top electrode. The samples were excited with a power of 50 μW at 400 nm by the second harmonic of a mode-locked Ti-Sapphire (Mira 900) laser delivering pulses of 150 fs at a repetition rate set using a pulse picker. All measurements were performed in a nitrogen-filled sample holder. Spectra were collected using a Hamamatsu *em*-CCD camera. The same excitation was used for time-resolved measurements and traces were instead collected with a Hamamatsu streak camera working in single-sweep mode. All spectra were corrected for the response of the instrument using a calibrated lamp.

4.3.5 Morphological Characterization

Samples for these measurements were prepared in the same way as those for PL measurements. AFM topographical images were recorded in tapping mode using a

Bruker Multimode 8 microscope with TESP probes; while SEM images were recorded on an XL 30 ESEM microscope.

References

[1] G. Xing, N. Mathews, S. Sun, S. S. Lim, Y. M. Lam, M. Graẗzel, S. Mhaisalkar, T. C. Sum, *Science* **2013**, *342*, 344.

[2] S. D. Stranks, G. E. Eperon, G. Grancini, C. Menelaou, M. J. P. Alcocer, T. Leijtens, L. M. Herz, A. Petrozza, H. J. Snaith, *Science* **2013**, *342*, 341.

[3] J. M. Ball, S. D. Stranks, M. T. Hörantner, S. Hüttner, W. Zhang, E. J. W. Crossland, I. Ramirez, M. Riede, M. B. Johnston, R. H. Friend, H. J. Snaith, *Energy Environ. Sci.* **2015**, *8*, 602.

[4] D. Sapori, M. Kepenekian, L. Pedesseau, C. Katan, J. Even, *Nanoscale* **2016**, *8*, 6369.

[5] M. A. Loi, J. C. Hummelen, *Nat Mater* **2013**, *12*, 1087.

[6] H. J. Snaith, A. Abate, J. M. Ball, G. E. Eperon, T. Leijtens, K. Nakita, S. D. Stranks, J. T. Wang, K. Wojciechowski, W. Zhang, *J. Phys. Chem. Lett.* **2014**, *5*, 1511.

[7] E. L. Unger, E. T. Hoke, C. D. Bailie, W. H. Nguyen, A. R. Bowring, T. Heumüller, M. G. Christoforo, M. D. McGehee, *Energy Environ. Sci.* **2014**, *7*, 3690.

[8] S. D. Stranks, V. M. Burlakov, T. Leijtens, J. M. Ball, A. Goriely, H. J. Snaith, *Phys. Rev. Appl.* **2014**, *2*, 1.

[9] S. Shao, M. Abdu-Aguye, L. Qiu, L.-H. Lai, J. Liu, S. S. Adjokatse, F. Jahani, M. E. Kamminga, G. H. ten Brink, T. Palstra, B. J. Kooi, J. C. Hummelen, M. A. Loi, *Energy Environ. Sci.* **2016**, *9*, 2444.

[10] Y. Deng, Z. Xiao, J. Huang, *Adv. Energy Mater.* **2015**, *5*, 1500721.

[11] R. Gottesman, E. Haltzi, L. Gouda, S. Tirosh, Y. Bouhadana, A. Zaban, E. Mosconi, F. De Angelis, *J. Phys. Chem. Lett.* **2014**, *5*, 2662.

[12] J.-H. Im, H.-S. Kim, N.-G. Park, *Cit. APL Mater.* **2014**, *2*, 81510.

[13] A. Dualeh, N. Tétreault, T. Moehl, P. Gao, M. K. Nazeeruddin, M. Grätzel, *Adv. Funct. Mater.* **2014**, *24*, 3250.

[14] F. Wang, H. Yu, H. Xu, N. Zhao, *Adv. Funct. Mater.* **2015**, *25*, 1120.

[15] N. Joong Jeon, J. Hong Noh, Y. Chan Kim, W. Seok Yang, S. Ryu, S. Il Seok, *Nat. Mater.* **2014**, *13*, 897.

[16] J. Hyuck Heo, H. J. Han, D. Kim, T. K. Ahn, S. H. Im, *Energy Environ. Sci.* **2015**, *8*, 1602.

[17] P.-W. Liang, C.-Y. Liao, C.-C. Chueh, F. Zuo, S. T. Williams, X.-K. Xin, J. Lin, A. K.-Y. Jen, *Adv. Mater.* **2014**, *26*, 3748.

[18] S. Bai, Z. Yuan, F. Gao, *J. Mater. Chem. C* **2016**, *4*, 3898.

[19] W.-J. Yin, T. Shi, Y. Yan, *Appl. Phys. Lett* **2014**, *104*, 63903.

[20] C. Bi, Y. Shao, Y. Yuan, Z. Xiao, C. Wang, Y. Gao, J. Huang, *J. Mater. Chem. A* **2014**, *2*, 18508.

[21] X. Huang, K. Wang, C. Yi, T. Meng, X. Gong, *Adv. Energy Mater.* **2016**, *6*, 1.

[22] S. Shao, Z. Chen, H.-H. Fang, G. H. Ten Brink, D. Bartesaghi, S. Adjokatse, L. J. A. Koster, B. J. Kooi, A. Facchetti, M. A. Loi, *J. Mater. Chem. A* **2016**, *4*, 2419.

[23] H. Wei, Y. Fang, P. Mulligan, W. Chuirazzi, H.-H. Fang, C. Wang, B. R. Ecker, Y. Gao, M. A. Loi, L. Cao, J. Huang, *Nat. Photonics* **2016**, *10*, 333.

[24] A. Walsh, D. O. Scanlon, S. Chen, X. G. Gong, S. H. Wei, *Angew. Chemie - Int. Ed.* **2015**, *54*, 1791.

[25] C. Eames, J. M. Frost, P. R. F. Barnes, B. C. O'Regan, A. Walsh, M. S. Islam, *Nat. Commun.* **2015**, *6*, 2.

[26] Y. Li, Y. Zhao, Q. Chen, Y. Yang, Y. Liu, Z. Hong, Z. Liu, Y. T. Hsieh, L. Meng, Y. Li, Y. Yang, *J. Am. Chem. Soc.* **2015**, *137*, 15540.

[27] C. Zhao, B. Chen, X. Qiao, L. Luan, K. Lu, B. Hu, *Adv. Energy Mater.* **2015**, *5*, 1.

[28] J. M. Azpiroz, E. Mosconi, J. Bisquert, F. De Angelis, *Energy Environ. Sci.* **2015**, *8*, 2118.

[29] M. Samiee, S. Konduri, B. Ganapathy, R. Kottokkaran, H. A. Abbas, A. Kitahara, P. Joshi, L. Zhang, M. Noack, V. Dalal, *Appl. Phys. Lett* **2014**, *105*, 153502.

[30] D. Shi, V. Adinolfi, R. Comin, M. Yuan, E. Alarousu, A. Buin, Y. Chen, S. Hoogland, A. Rothenberger, K. Katsiev, Y. Losovyj, X. Zhang, P. A. Dowben, O. F. Mohammed, E. H. Sargent, O. M. Bakr, *Science* **2015**, *347*, 519.

[31] L. J. A. Koster, S. E. Shaheen, J. C. Hummelen, *Adv. Energy Mater.* **2012**, *2*, 1246.

[32] Q. Lin, A. Armin, R. C. R. Nagiri, P. L. Burn, P. Meredith, *Nat. Photonics* **2015**, *9*, 106.

[33] V. D'Innocenzo, G. Grancini, M. J. P. Alcocer, A. R. S. Kandada, S. D. Stranks, M. M. Lee, G. Lanzani, H. J. Snaith, A. Petrozza, *Nat. Commun.* **2014**, *5*, 3586.

[34] H.-H. Fang, R. Raissa, M. Abdu-Aguye, S. Adjokatse, G. R. Blake, J. Even, M. A. Loi, *Adv. Funct. Mater.* **2015**, *25*, 2378.

[35] M. Kuik, L. J. A. Koster, G. A. H. Wetzelaer, P. W. M. Blom, *Phys. Rev. Lett.* **2011**, *107*, 1.

[36] T. S. Sherkar, L. J. A. Koster, *ACS Appl. Mater. Interfaces* **2015**, *7*, 11881.

[37] F. Jahani, S. Torabi, R. C. Chiechi, L. J. A. Koster, J. C. Hummelen, L. Jan, A. Koster, J. C. Hummelen, *Chem. Commun.* **2014**, *50*, 10645.

[38] S. Torabi, F. Jahani, I. Van Severen, C. Kanimozhi, S. Patil, R. W. A. Havenith, R.

C. Chiechi, L. Lutsen, D. J. M. Vanderzande, T. J. Cleij, J. C. Hummelen, L. J. A. Koster, *Adv. Funct. Mater.* **2015**, *25*, 150.

[39] S. R. Cowan, R. A. Street, S. Cho, A. J. Heeger, *Phys. Rev. B - Condens. Matter Mater. Phys.* **2011**, *83*, 1.

[40] G. J. A. H. Wetzelaer, M. Scheepers, A. M. Sempere, C. Momblona, J. Ávila, H. J. Bolink, *Adv. Mater.* **2015**, *27*, 1837.

[41] R. L. Milot, G. E. Eperon, H. J. Snaith, M. B. Johnston, L. M. Herz, *Adv. Funct. Mater.* **2015**, *25*, 6218.

[42] N. K. Noel, A. Abate, S. D. Stranks, E. Parrott, V. Burlakov, A. Goriely, H. J. Snaith, *Nano* **2014**, *8*, 9815.